

Reversible quantum information spreading in many-body systems near criticality

Quirin Hummel, Benjamin Geiger, Juan Diego Urbina, and Klaus Richter
Institut für Theoretische Physik, Universität Regensburg, D-93040 Regensburg, Germany
(Dated: December 15, 2024)

Quantum chaotic interacting N -particle systems are assumed to show fast and irreversible spreading of quantum information on short (Ehrenfest) time scales $\sim \log N$. Here we show that, near criticality, certain many-body systems exhibit fast initial scrambling, followed subsequently by oscillatory behavior between reentrant localization and delocalization of information in Hilbert space. Specifically, we consider quantum critical bosonic systems with attractive contact interaction that, despite being integrable, exhibit locally unstable dynamics in the corresponding many-body phase space of the large- N limit. Semiclassical quantization of the latter accounts for many-body correlations in excellent agreement with simulations. Most notably, it predicts an asymptotically constant local level spacing \hbar/τ , again given by $\tau \sim \log N$. This governs the long-time behavior of out-of-time-order correlators that feature quasi-periodic recurrences indicating reversibility.

The dynamics of quantum information in complex many-body (MB) systems presently attracts a lot of attention [1, 2] ranging from atomic and condensed quantum matter to high energy physics. The evolution of an (excited) quantum MB system towards a state of thermal equilibrium usually goes along with the scrambling of quantum correlations, encoded in the initial state, across the systems's many degrees of freedom. Understanding such dynamics requires an improved understanding of MB quantum chaos, its links with thermalization [3–6] and the suppression of the latter [1, 7, 8], including the role of non-classicality in MB physics.

Echo protocols, measuring how a perturbation affects successive forward and backward propagations in time, sensitively probe the stability of complex quantum dynamics. In this respect out-of-time-order correlators (OTOCs) [9–11] $C(t) = \langle [\hat{W}(t), \hat{V}]^\dagger [\hat{W}(t), \hat{V}] \rangle$ based on commutators of operators \hat{V}, \hat{W} play a central role in exploring the various features of quantum thermalization and chaos with first experimental implementations [12–14].

The OTOC time evolution allows one to distinguish various classes of MB systems by their operator growth. On the one side there are slow scramblers, such as systems in the MB localized phase exhibiting logarithmically slow operator spreading [15–18] or, e.g., Luttinger liquids [19] showing only quadratic increase. On the other side, an exponentially fast initial growth of OTOCs is commonly viewed as a quantum signature of MB chaotic behavior. Corresponding examples comprise systems with holographic duals to black holes [10, 20], the SYK-model [11, 21–23], and condensed matter systems close to a quantum phase transition [24–27] or exhibiting chaos in the classical limit of large particle number N . In such large- N systems, the exponential growth rate for OTOCs is given by the Lyapunov exponent of their classical counterpart [10, 27–33] and prevails up to the Ehrenfest $\log N$ time where MB quantum interference sets in [32, 34]. The subsequent OTOC time evolution towards an ergodic limit is then often governed by relaxation through

slow classical modes [35].

Here we show that exponentially fast scrambling need not necessarily lead to quantum information loss: There exist systems exhibiting initial growth of complexity without relaxation, i.e., after a quench to an interacting system close to criticality the OTOCs do not show monotonous saturation; instead the correlations imprinted initially can be periodically retrieved.

Large- N quantum critical systems are particularly suited for considering the inter-relation between spreading of correlations, quantified through OTOCs, and corresponding nonlinear classical mean-field (MF) dynamics. In such systems critical phenomena are often viewed as quantum manifestations of structural changes in classical phase space, associated with unstable MF motion close to separatrices. While corresponding studies [36–42] commonly invoke a classical MF analysis, we will show that MB semiclassical quantization beyond MF allows for an essentially exact characterization of the locally unstable quantum dynamics.

Specifically, in generic quantum chaotic systems, the Ehrenfest time $\sim \log N$ is distinctly shorter than the Heisenberg time which is usually algebraic in N and associated with the inverse mean level spacing. On the contrary, as we will show, these two scales coincide for certain quantum critical systems. Quantization of their locally hyperbolic MB dynamics implies two inter-related features: Even though the dynamics may be separable, OTOCs still grow exponentially with a rate given by the local MF instability exponent λ_s up to times $(1/\lambda_s) \log N$. Second, the inverse mean level spacing in the relevant spectral region also scales as $\log N$. Hence, this type of quantum critical dynamics is governed by $\log N$ as the sole time scale.

Remarkably, this level spacing, the spectral gap, turns out to be asymptotically constant, i.e., approaching the spectrum of a harmonic oscillator, although the underlying hyperbolic dynamics is unstable and rather corresponds to an inverted oscillator [43]. This equidistant level spacing implies uniquely strong, periodic quantum

recurrences on short $\log N$ -scales that dominate OTOCs and hence reflect *unscrambling* of quantum information in a quantum critical MB system. On the contrary, in chaotic MB systems randomlike evolution is expected for enormously long (Heisenberg) times beyond which the spectral discreteness eventually enforces recurrences [44].

A generic example of critical behavior is the 1D attractive Bose gas with periodic boundary conditions (attractive Lieb-Liniger model) [45–47]. While its Hamiltonian

$$\hat{\mathcal{H}} = - \int_0^{2\pi} d\theta \hat{\Psi}^\dagger(\theta) \partial_\theta^2 \hat{\Psi}(\theta) + \frac{\pi\tilde{\alpha}}{2} [\hat{\Psi}^\dagger(\theta)]^2 [\hat{\Psi}(\theta)]^2, \quad (1)$$

with bosonic field operators $\hat{\Psi}$ and $\hat{\Psi}^\dagger$, realistically describes quasi-1D ultracold gases of bosonic atoms with interactions parametrized by $\tilde{\alpha}$ [48–50], its MF dynamics is governed by the Gross-Pitaevskii equation. It exhibits a quantum phase transition (QPT) at a critical coupling $\tilde{\alpha}N = 1$ [46, 51, 52] where the homogeneous condensate starts forming a bright soliton. Although for finite N the spectrum of the quantum integrable Hamiltonian (1) can be, in principle, found through Bethe ansatz [47, 53], this does not allow for systematically treating the $N \rightarrow \infty$ limit, except for special states [54, 55]. Instead we truncate (see Appendix A) the field operators to the lowest three momentum modes

$$\hat{\Psi}(\theta) = (\hat{a}_0 + \hat{a}_{-1}e^{-i\theta} + \hat{a}_1e^{i\theta})/\sqrt{2\pi}, \quad (2)$$

as commonly done for exact diagonalization [51, 56, 57]—a good approximation for $\tilde{\alpha}N < 1$ that also contains all the physics relevant for the understanding of the QPT and its precursors for $\tilde{\alpha}N \geq 1$ [46, 47, 52, 56]. The model (1,2) near the QPT has recently served to mimic black holes as graviton condensates [56, 58]. Furthermore, despite the truncation introducing long-range interactions, this system can be essentially realized using ultracold spin-1 atoms [59] and has attracted considerable attention [60–62] also as model for time crystals [63].

Besides the energy also particle number $\hat{N} = \sum_k \hat{a}_k^\dagger \hat{a}_k$ and total (angular) momentum $\hat{K} = \sum_k k \hat{a}_k^\dagger \hat{a}_k$ are conserved. Hence, the truncation to three modes, in contrast to five or more modes [64], renders the system integrable in that its large- N MF limit, formally representing a classical limit, is integrable. The integrable MF dynamics allows for devising a MB version of semiclassical torus quantization [65, 66] to analytically find the spectrum and wave functions that are asymptotically exact for $N \rightarrow \infty$. To this end we write the operators in symmetric order and replace $\hat{a}_k \mapsto \sqrt{n_k}e^{i\vartheta_k}$ for $k = -1, 0, 1$, where (n_k, ϑ_k) are continuous classical conjugate variables. Using $\tilde{N} \equiv n_{-1} + n_0 + n_1$ and $\tilde{K} \equiv n_1 - n_{-1}$ and considering $\tilde{K} = 0$ the classical energy per particle is (see Appendix B), defining the scaled interaction $\alpha = \tilde{\alpha}\tilde{N}$,

$$\frac{E}{\tilde{N}} = \omega(z, \varphi) + \frac{3\alpha}{2\tilde{N}} - \frac{9\alpha}{8\tilde{N}^2} - \frac{1}{\tilde{N}} - \frac{\alpha}{4}, \quad (3)$$

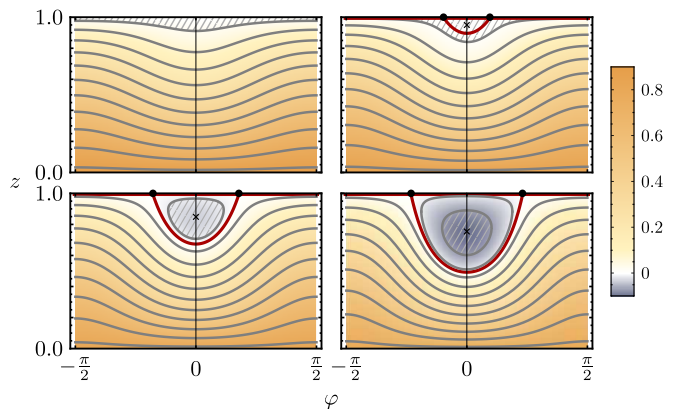


FIG. 1. Phase space portrait of energy $\omega(z, \varphi)$, Eq. (4), where z denotes the relative occupation of the noninteracting ground state and φ the conjugate angle, for different values of interaction α . Gray lines represent the orbits (tori) that fulfill the quantization condition (6) for $N = 20$. For $\alpha > 1$, two hyperbolic fixed points (dots at $z = 1$) and a global energy minimum (cross) appear. Upper left panel: $\alpha = 0.8$, no separatrix. Upper right: $\alpha = 1.1$, separatrix (red) exists, only quantized rotations. Lower left: $\alpha = 1.4$, one quantized vibration (ground state). Lower right: $\alpha = 1.8$, two quantized vibrations.

where the classical dynamics is completely determined by

$$\omega(z, \varphi) = (1 - z) [1 - \alpha [(1 - z)/8 + z \cos^2 \varphi]] \quad (4)$$

with phase space coordinates

$$z = \frac{n_0}{\tilde{N}}, \quad \varphi = \vartheta_0 - \frac{\vartheta_1 + \vartheta_{-1}}{2}, \quad \{z, \varphi\} = \frac{1}{\tilde{N}}. \quad (5)$$

The Poisson bracket $\{\cdot, \cdot\}$ is defined by (n_0, φ) . The transformation $(E, n_0, \varphi) \mapsto (\omega, z, \varphi)$ renders the classical dynamics independent of \tilde{N} , while introducing the effective quantum of action $\hbar_{\text{eff}} = 1/\tilde{N}$ [67].

The effective Hamiltonian $\omega(z, \varphi)$ gives rise to different types of classical trajectories following lines of constant energy in phase space with periodicity $\varphi \mapsto \varphi + \pi$, see Fig. 1. For $\alpha < 1$ all trajectories are deformed horizontal lines (rotations). For $\alpha > 1$ an island centered around a new minimum energy fixed point emerges with trajectories vibrating in φ . This goes along with the formation of a separatrix at $E = E_{\text{sep}}$ ($\omega = 0$) associated with two hyperbolic fixed points at $z = 1$ and characterized by (in)stability exponents $\lambda_s^{(1,2)} = 2\sqrt{\alpha - 1} \equiv \lambda_s$.

In order to study genuine quantum effects we go beyond the classical MF picture by means of semiclassical torus quantization. Related WKB approaches successfully used in two-site models [68–70] would miss topological aspects (arising from reducing the full phase space to a single degree of freedom) that affect MB interference. These appear as (half-integer) Maslov indices [66] in the

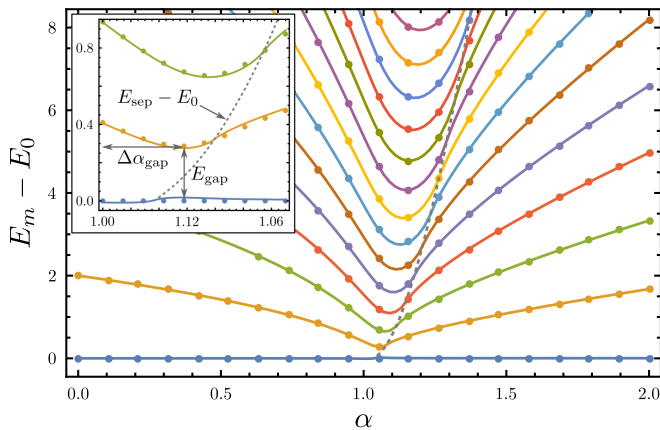


FIG. 2. Excitation spectrum $E_m - E_0$ for $m = 0, 1, 2, \dots, N = 300$ and $0 \leq \alpha \leq 2$. Both numerical (symbols) and semiclassical (lines) excitation spectra were calculated with respect to the numerical ground state energy. The gray dotted line indicates inflection points where quantized orbits cross the separatrix (in Fig. 1). Inset: closeup around $\alpha=1$.

quantization rules

$$\frac{1}{2\pi} \oint d\varphi [1 - z(\omega, \varphi)] = \frac{m + \frac{1}{2}}{\tilde{N}}, \quad (6)$$

$$m = 0, 1, \dots, \lfloor N/2 \rfloor, \quad \tilde{N} = N + 3/2, \quad N = 0, 1, \dots$$

Equations (6) effectively quantize the phase space areas bounded by the lines $\omega = \text{const.}$ (shaded areas in Fig. 1 for $m = 0$), giving rise to quantized energies ω_m and E_m in perfect agreement with results from exact diagonalization, as demonstrated in Fig. 2 for $N=300$.

The QPT in the limit $N \rightarrow \infty$ is associated with the ground state corresponding to the quantized orbit enclosing the phase space area $1/(2\tilde{N}) \rightarrow 0$ that is always vibrational for $\alpha > 1$ if \tilde{N} is large enough. Its energy scales as $\omega_{\min} \sim -(\alpha - 1)^2$, in contrast to $\omega_{\min} = 0$ for $\alpha < 1$ where the quantized orbit approaches the line $z = 1$, giving rise to the nonanalytic dependence on α of the MF ground state at $\alpha=1$. Precursors of such nonanalyticity for finite \tilde{N} can be identified for every quantized orbit changing from rotation to vibration upon tuning α . This is reflected in the sequence of avoided crossings in Fig. 2 building up an excited-state QPT (ES-QPT) when $\tilde{N} \rightarrow \infty$ [37, 40]. Remarkably, the semiclassical quantization (6) even allows us (see Appendix C) to analytically obtain the scaling laws governing the approach of $\Delta\alpha_{\text{gap}} \sim N^{-2/3}$ and $E_{\text{gap}} \sim N^{-1/3}$ (see inset) to their MF values, in perfect agreement with numerical and heuristic observations [46, 51, 57].

Hence, MB semiclassical quantization goes beyond the quasiparticle Bogoliubov picture of [46, 52] where the excitation spectrum collapses to zero at the MF critical coupling $\alpha=1$. Instead, for finite \tilde{N} we find a huge accumulation of levels around the separatrix. This precursor of an ESQPT gives rise to characteristic features in the

spectral properties and to the emergence of a *local log time scale*. To see this, an asymptotic $N \gg 1$ analysis (see Appendix D) suggests a separation into a dominant, local action contribution by quadratic expansion at the fixed points and a non-local correction from linearization around sections of the separatrix. The asymptotic analysis for (6) (see Appendix E for the application to the model) yields the average density of states

$$\bar{\rho}(E) = \frac{-1}{2\pi\lambda} \log\left(\frac{|E - E_{\text{sep}}|}{\tilde{N}}\right) + \frac{t_{\text{sep}}}{2\pi} + \mathcal{O}\left(\frac{E - E_{\text{sep}}}{N^2}\right) \quad (7)$$

with a characteristic logarithmic divergence at $E = E_{\text{sep}}$ (see Fig. 3). Here $\lambda = \lambda_s/2 = \sqrt{\alpha - 1}$ is given by the exponents of the hyperbolic fixed points, and $t_{\text{sep}} = (\alpha - 1)^{-1/2} \log[128(\alpha - 1)^2/(\alpha^2(8 - \alpha))]$ is the regularized part of the separatrix traversal time between fixed points. Evaluating (6) around the separatrix, equivalent to quantization $\int_{E_{\text{sep}}}^{E_{[k]}} dE' \bar{\rho}(E') = \mu + k$, gives

$$E_{[k]} \approx \frac{-2\pi\lambda(\mu + k)}{\mathcal{W}_{-1}(-2\pi\lambda/\tilde{N}e^{-1-\lambda t_{\text{sep}}|\mu + k|})}, \quad k \in \mathbb{Z}. \quad (8)$$

Here $E_{[0]}$ refers to the first level larger than E_{sep} (its exact position determined by an index shift $\mu \in [0, 1]$), and \mathcal{W}_{-1} is the lower branch of the Lambert- \mathcal{W} function [71].

Most notably, close to the logarithmic divergence of $\bar{\rho}(E)$ one finds (see Appendix F) from (8) that a set of levels, growing in number logarithmically with N , becomes *asymptotically equidistant* with level spacing ΔE , as shown in Fig. 4. The associated time scale (see Appendix G)

$$\tau = \frac{2\pi}{\Delta E} = \frac{1}{\lambda} \log \tilde{N} + \mathcal{O}(1) \quad (9)$$

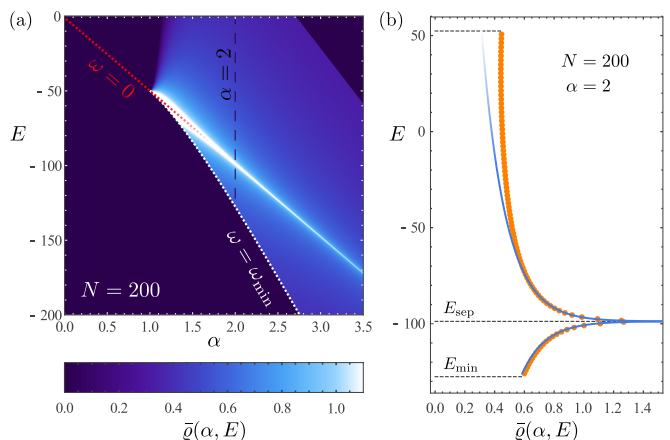


FIG. 3. (a) Asymptotic density of states $\bar{\rho}(\alpha, E)$, Eq. (7), showing level bunching (bright straight line) around the finite size precursor of the excited-states quantum phase transition at $E = E_{\text{sep}}$ in the supercritical regime $\alpha > 1$. (b) Slice of $\bar{\rho}(\alpha, E)$ at $\alpha = 2$ in comparison with numerically calculated inverse level gaps (orange symbols).

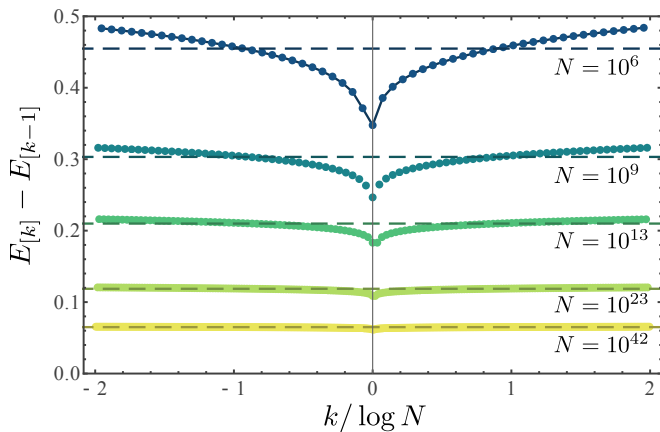


FIG. 4. Asymptotic level spacings $E_{[k]} - E_{[k-1]}$, Eq. (8), (symbols) between states near the separatrix approaching the characteristic constant spacing ΔE , Eq. (9), (dashed) for $\alpha = 2$ and $N = 10^6, 10^9, 10^{13}, 10^{23}, 10^{42}$ (the latter with relevance for black hole physics) from top/blue to bottom/yellow within windows with $\sim \log N$ levels. Energies obtained from the full semiclassical quantization, Eq. (6), (solid line) for $N = 10^6$ confirm the validity of Eq. (8).

is the Heisenberg time corresponding to the local spectral gap ΔE , but exhibits a striking similarity with the Ehrenfest time $\tau_E = (1/\lambda_L) \log \hbar_{\text{eff}}^{-1}$ with $\hbar_{\text{eff}} = \hbar$ and $1/\tilde{N}$ in chaotic single-particle [72], respectively, MB systems [32] with Lyapunov exponent λ_L . This justifies to interpret the leading order of (9) also as a *local Ehrenfest time* associated with the dynamical instability characteristic of critical behavior. This crossover of the Heisenberg time from usually being algebraic in N to log time behavior is not shared by generic chaotic systems.

In the following we address the drastic consequences of this transition for the evolution of quantum MB correlations: We quantify the spreading of information through the OTOC

$$C(t) = -N^{-4} \langle \psi | [\hat{n}_0(0), \hat{n}_0(t)]^2 | \psi \rangle \quad (10)$$

based on the operators $\hat{n}_0(t)/N$ of the normalized ground state occupation. For chaotic systems quasi-classical arguments [9, 10, 28] confirmed by MB semiclassical theory [32] predict a short-time behavior $C(t) \sim \hbar^2 e^{2\lambda_L t}$ passing into a saturation regime at τ_E . Despite the fact that the system (2) is integrable, we can use similar arguments to predict that in the quantum critical regime the dynamical instability close to the hyperbolic fixed points also causes such an exponential behavior,

$$C(t) \sim (\hbar_{\text{eff}}^2 / \tilde{N}^2) e^{2\lambda_s t}, \quad (11)$$

but with a rate given instead by the (in)stability exponents λ_s (see [42] for a related result for chains of large spins). The prefactor $1/\tilde{N}^2$ in (11) stems from the choice of the initial state.

Contrary to non-integrable MB systems considered so far in the literature, within the present MB model we

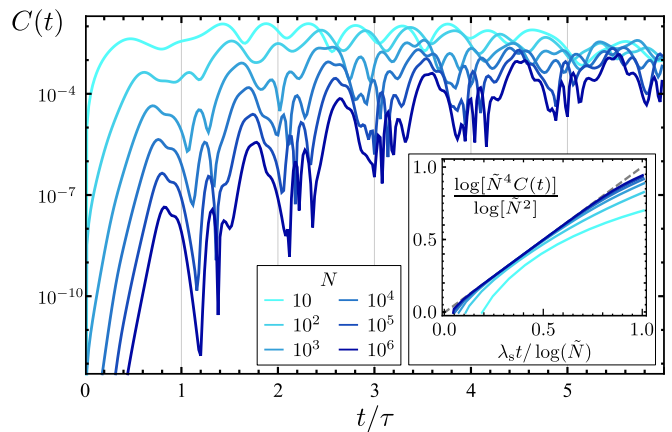


FIG. 5. Oscillatory time evolution of the out-of-time-order correlator (10), reflecting scrambling and unscrambling close to criticality for various particle numbers N (at $\alpha = 2.0$). $C(t)$ exhibits approximately τ -periodic oscillations (including finite size corrections, see Appendix G) where τ , Eq. (9), is the local Ehrenfest time. Inset: Initial growth of $C(t)$ approaching the exponent $2\lambda_s t$ (marked as dashed line in the log plot) with increasing N , thereby confirming Eq. (11).

have numerical access to huge particle numbers and hence can thoroughly check the commonly assumed exponential growth of OTOCs in the truly semiclassical large- N limit, as well as associated log-time effects. In Fig. 5 we present numerical results for $C(t)$ computed from (10) after imposing an interaction quench to the initial non-interacting ground state $|\psi\rangle = 1/\sqrt{N!} (a_0^\dagger)^N |0\rangle$, such that the dynamics is dominated by states close to E_{sep} (see Appendix G). In the inset the short time behavior of $\log C(t)$ up to the local Ehrenfest time scale $\tau_E = (1/\lambda_s) \log N$ is displayed for particle numbers ranging from $N = 10^2$ to 10^6 , indeed showing convergence to the slope $2\lambda_s t$ (dashed line) predicted in (11).

For $t > \tau_E$ a saturation of OTOCs, monotonously approaching a plateau at late times, is characteristic for generic chaotic MB systems. Instead, as shown in Fig. 5, $C(t)$ exhibits distinct oscillations with a period given by the log time τ , (9), that includes finite-size corrections (see Appendix G) and hence slightly differs from τ_E . Since $C(t)$ is a measure of information spreading, these oscillations reflect reversibility of quantum information flux in Hilbert space as a result of genuine MB interference. This is further supplemented by corresponding oscillations in the associated evolution of entanglement, e.g., encoded in the one-body entropy (see Appendix G). We trace these observations back to the fact that, close to criticality, $C(t)$ is dominated by an increasing (with $\log N$) number of states sufficiently close to E_{sep} (see Appendix G) where the spectrum gets asymptotically equidistant (Fig. 4). This induces revivals (getting more and more pronounced with increasing N) associated with the unique time scale, the log time τ , (9), that

takes the role of a Heisenberg time close to criticality. To clearcut show this asymptotic periodicity, here deduced from semiclassical MB separatrix quantization, requires large N in regimes that, to the best of our knowledge, are not accessible with present numerical methods for chaotic MB systems.

In conclusion, by means of many-body semiclassical quantization we could explain the exponentially fast scrambling and buildup of correlations in quantum systems that are critical, but not globally chaotic. We uncovered a mechanism for fast dynamics near a quantum critical point where the Heisenberg time takes the role of a short Ehrenfest-type log-time scale. Moreover, for large N we have demonstrated the emergence of nearly

equidistant spectra that in turn give rise to recurrences in OTOCs on $\log N$ -time scales. Such periodic features resemble those of time crystals [63]. We believe such memory effects to exist in larger classes of critical systems with a dynamical decoupling of a dominant unstable mode from other collective degrees of freedom. Their observation should be in experimental reach since, e.g., recurrences based on stable dynamics have already been observed in a system with thousands of atoms [73]. Moreover, our results shed light on generic mechanisms governing the dynamics of correlations at (excited-state) quantum phase transitions beyond mean field.

We acknowledge funding through the Studienstiftung des Deutschen Volkes (BG) and the Deutsche Forschungsgemeinschaft through project Ri681/14-1.

Appendix

Appendix A: The truncated model

The starting point is the Hamiltonian for bosons on a ring with attractive ($\tilde{\alpha} \geq 0$) contact interaction formulated in second quantization [74]

$$\hat{H} = \int_0^{2\pi} d\theta \left[-\hat{\psi}^\dagger(\theta) \partial_\theta^2 \hat{\psi}(\theta) - \frac{\pi \tilde{\alpha}}{2} \hat{\psi}^\dagger(\theta) \hat{\psi}^\dagger(\theta) \hat{\psi}(\theta) \hat{\psi}(\theta) \right], \quad (\text{A2})$$

where the field operators $\hat{\psi}^\dagger(\theta)$ and $\hat{\psi}(\theta)$ are creation and annihilation operators of bosons at position θ with periodic identification $\hat{\psi}(\theta + 2\pi) = \hat{\psi}(\theta)$ and obeying the bosonic commutation relations

$$\begin{aligned} [\hat{\psi}(\theta), \hat{\psi}(\theta')] &= [\hat{\psi}^\dagger(\theta), \hat{\psi}^\dagger(\theta')] = 0, \\ [\hat{\psi}(\theta), \hat{\psi}^\dagger(\theta')] &= \delta(\theta - \theta'), \end{aligned} \quad (\text{A3})$$

making use of the restriction of θ to one specific interval of length 2π . The form (A2) corresponds to the Lieb-Liniger model [45] when setting units by $\frac{\hbar^2}{2m} = 1$ and $L = 2\pi$. In other words, energy will be given in units of

$$[E] = \frac{4\pi^2 \hbar^2}{2mL^2}, \quad (\text{A4})$$

where L is the length of the system. Similarly the coupling parameter is related to the two-body scattering length a_{3D} (which is negative for attractive interactions considered here) by [75]

$$\tilde{\alpha} = -\frac{2m}{\pi^2 \hbar} L a_{3D} \omega_\perp, \quad (\text{A5})$$

when applied to realistic ultracold quasi-1D Bose gases in the regime $a_{3D} \ll \sqrt{\hbar/m\omega_\perp}$ of strong transversal confinement with trapping frequency ω_\perp . Eq. (A2) also admits to account for confinement induced resonances [75]

by a modification of (A5). We do not take into account effective three-body interaction due to finite confinement and the consequent existence of excited trimer states reported in [76–78].

By Fourier decomposition of the field operators into momentum modes

$$\hat{\psi}(\theta) = \frac{1}{\sqrt{2\pi}} \sum_{k \in \mathbb{Z}} e^{ik\theta} \hat{a}_k, \quad (\text{A6})$$

where the annihilation and creation operators in the momentum modes fulfill

$$\begin{aligned} [\hat{a}_k, \hat{a}_l] &= [\hat{a}_k^\dagger, \hat{a}_l^\dagger] = 0, \\ [\hat{a}_k, \hat{a}_l^\dagger] &= \delta_{kl}, \end{aligned} \quad (\text{A7})$$

the Hamiltonian (A2) reads

$$\hat{H} = \sum_{k \in \mathbb{Z}} k^2 \hat{a}_k^\dagger \hat{a}_k - \frac{\tilde{\alpha}}{4} \sum_{k,l,m,n \in \mathbb{Z}} \delta_{k+l,m+n} \hat{a}_k^\dagger \hat{a}_l^\dagger \hat{a}_m \hat{a}_n. \quad (\text{A8})$$

Truncating the Hilbert space to the three lowest single particle momentum modes $k = -1, 0, 1$, or, equivalently, neglecting the occupation of high modes $|k| \geq 2$ by setting them to zero, yields

$$\hat{H}_3 = \sum_{k=-1}^1 k^2 \hat{a}_k^\dagger \hat{a}_k - \frac{\tilde{\alpha}}{4} \sum_{k,l,m,n=-1}^1 \delta_{k+l,m+n} \hat{a}_k^\dagger \hat{a}_l^\dagger \hat{a}_m \hat{a}_n. \quad (\text{A9})$$

The validity of this truncation comes from the relevance of low momentum modes for the quantum phase transition [47, 51, 52] and goes far beyond a perturbative expansion in powers of $\tilde{\alpha}$. One can easily show that

$$\begin{aligned} [\hat{H}_3, \hat{N}] &= 0, \\ [\hat{H}_3, \hat{K}] &= 0, \end{aligned} \quad (\text{A10})$$

with the total number of particles and momentum operator

$$\begin{aligned}\hat{N} &= \sum_{k \in \{-1, 0, 1\}} \hat{a}_k^\dagger \hat{a}_k, \\ \hat{K} &= \sum_{k \in \{-1, 0, 1\}} k \hat{a}_k^\dagger \hat{a}_k = \hat{a}_1^\dagger \hat{a}_1 - \hat{a}_{-1}^\dagger \hat{a}_{-1}.\end{aligned}\quad (\text{A11})$$

When a specific quantum state is considered, an indicator for the defect introduced due to the truncation (A9) is the depopulation of the single-particle ground state $k = 0$. If an eigenstate of (A9) in the truncated Hilbert space is merely slightly populated in the modes $k = \pm 1$, one can assume that the occupation of all truncated modes $|k| > 1$ in the corresponding exact eigenstate of the full Hamiltonian (A8) is even smaller and thus negligible. As concerns the QPT and the ESQPT relevant for scrambling and dynamics of interparticle correlations, the depletion of the condensate can be made arbitrarily small by increasing the number of particles, which allows to reduce $N\tilde{\alpha}$ arbitrarily close to the MF critical value of 1 and still stay in a sufficiently supercritical regime to fulfill all requirements necessary for the analysis.

Appendix B: The classical limit

In order to obtain the classical counterpart of the truncated quantum system, one has to replace the creation and annihilation operators by complex valued classical variables

$$\begin{aligned}\hat{a}_k &\mapsto \phi_k =: \frac{1}{\sqrt{2}}(q_k + ip_k), \\ \hat{a}_k^\dagger &\mapsto \phi_k^* =: \frac{1}{\sqrt{2}}(q_k - ip_k),\end{aligned}\quad (\text{B2})$$

with the new classical coordinates q_k and canonically conjugated momenta p_k that take real values. In addition special care has to be taken considering the ordering of operators. The correct prescription [79] thereby is to replace symmetrically ordered products of operators

$$\left\{ \hat{a}_{k_1} \cdots \hat{a}_{k_m} \hat{a}_{l_1}^\dagger \cdots \hat{a}_{l_n}^\dagger \right\}_{\text{sym}} \mapsto \phi_{k_1} \cdots \phi_{k_m} \phi_{l_1}^* \cdots \phi_{l_n}^*, \quad (\text{B3})$$

where the symmetric ordering is defined by the sum of all possible orderings divided by their number

$$\{\hat{c}_1 \cdots \hat{c}_n\}_{\text{sym}} := \frac{1}{n!} \sum_{\sigma \in S_n} \hat{c}_{\sigma(1)} \cdots \hat{c}_{\sigma(n)}, \quad (\text{B4})$$

where the c_j can be any creation and/or annihilation operators and σ runs over all permutations of n (summarized by the symmetric group S_n). Ordering the operators in (A9) using (A7) and performing the prescription (B3) yields the classical Hamilton function for the truncated

Lieb-Liniger model

$$\begin{aligned}H_{\text{cl}} &= \sum_k \left(k^2 + \frac{3\tilde{\alpha}}{2} \right) |\phi_k|^2 \\ &\quad - \frac{\tilde{\alpha}}{4} \sum_{k,l,m,n} \delta_{k+l,m+n} \phi_k^* \phi_l^* \phi_m \phi_n - \frac{9\tilde{\alpha}}{8} - 1,\end{aligned}\quad (\text{B5})$$

where the specification of the index sets in the sums has been omitted in order to ease notation.

The canonical transformation

$$\begin{aligned}\frac{1}{\sqrt{2}}(q_k + ip_k) &\mapsto \sqrt{n_k} e^{-i\vartheta_k} \\ n_k &\in \mathbb{R}^+, \vartheta_k \in [0, 2\pi]\end{aligned}\quad (\text{B6})$$

fulfills

$$\begin{aligned}\{\vartheta_k, \vartheta_l\}_{\mathbf{q}, \mathbf{p}} &= \{n_k, n_l\}_{\mathbf{q}, \mathbf{p}} = 0, \\ \{\vartheta_k, n_l\}_{\mathbf{q}, \mathbf{p}} &= \delta_{kl},\end{aligned}\quad (\text{B7})$$

with Poisson brackets

$$\{f, g\}_{\mathbf{q}, \mathbf{p}} := \sum_k \left(\frac{\partial f}{\partial q_k} \frac{\partial g}{\partial p_k} - \frac{\partial g}{\partial q_k} \frac{\partial f}{\partial p_k} \right). \quad (\text{B8})$$

Note that the transformation into polar coordinates (B6) introduces a punctuation of the (q_k, p_k) -planes, so that orbits or paths cannot continuously be deformed across these singularities using (ϑ_k, n_k) coordinates. This is especially important for the calculation of Maslov indexes [80] needed for the EBK quantization of the model.

The transformation brings the Hamilton function into the form

$$\begin{aligned}H_{\text{cl}} &= \sum_k \left(k^2 + \frac{3\tilde{\alpha}}{2} \right) n_k - \frac{9\tilde{\alpha}}{8} - 1 - \frac{\tilde{\alpha}}{4} [n_0^2 + n_1^2 + n_{-1}^2 \\ &\quad + 4(n_0 n_1 + n_0 n_{-1} + n_1 n_{-1}) \\ &\quad + 4n_0 \sqrt{n_1 n_{-1}} \cos(2\vartheta_0 - \vartheta_1 - \vartheta_{-1})].\end{aligned}\quad (\text{B9})$$

In addition to energy conservation $\frac{d}{dt} H_{\text{cl}} = \frac{\partial}{\partial t} H_{\text{cl}} = 0$ there exist two constants of motion

$$\tilde{N} = n_0 + n_{-1} + n_1, \quad (\text{B10})$$

$$\tilde{K} = n_1 - n_{-1},$$

$$\{\tilde{N}, H_{\text{cl}}\} = \{\tilde{K}, H_{\text{cl}}\} = 0, \quad (\text{B11})$$

closely related to the total number of particles N and the total momentum K as eigenvalues of (A11).

A further point transformation takes the phase space variables $(\vartheta_0, \vartheta_{-1}, \vartheta_1, n_0, n_{-1}, n_1)$ into $(\varphi, \varphi_N, \varphi_K, n_0, \tilde{N}, \tilde{K})$ given by

$$\varphi = \vartheta_0 - \frac{1}{2}(\vartheta_1 + \vartheta_{-1}),$$

$$\varphi_N = \frac{1}{2}(\vartheta_1 + \vartheta_{-1}), \quad (\text{B12})$$

$$\varphi_K = \frac{1}{2}(\vartheta_1 - \vartheta_{-1}),$$

leaves us with the expression

$$H_{\text{cl}} = (\tilde{N} - n_0) + \frac{3\tilde{\alpha}}{2}\tilde{N} - \frac{9\tilde{\alpha}}{8} - 1 - \frac{\tilde{\alpha}}{4} \left[\frac{3}{2}\tilde{N}^2 - \frac{3}{2}n_0^2 + n_0\tilde{N} - \frac{1}{2}\tilde{L}^2 + 2n_0\sqrt{(\tilde{N} - n_0)^2 - \tilde{L}^2(2\cos^2\varphi - 1)} \right]. \quad (\text{B13})$$

In the following we use scaled variables

$$z := \frac{n_0}{\tilde{N}}, \quad l := \frac{\tilde{K}}{\tilde{N}}, \quad \alpha := \tilde{\alpha}\tilde{N}, \quad (\text{B14})$$

where z is then closely related to the classical version of the (subcritical) condensate fraction and l is closely related to the average angular momentum per particle. These two relations will show up to become exact in the limit $N \rightarrow \infty$. Therefore, we refer to the two quantities as the mentioned notions, keeping in mind that they are not exactly correct for finite N . In these scaled variables the energy per particle reads [Eq. (3) of the main text],

$$\frac{H_{\text{cl}}}{\tilde{N}} = \omega(\varphi, z, l) - \frac{\alpha}{4} - \frac{1}{\tilde{N}} + \frac{3\alpha}{2\tilde{N}} - \frac{9\alpha}{8\tilde{N}^2} \quad (\text{B15})$$

where the classical dynamics is completely determined by

$$\omega(\varphi, z, l) = 1 - z - \frac{\alpha}{4} \left[\frac{1}{2} + z - \frac{3}{2}z^2 - \frac{1}{2}l^2 - 2z\sqrt{(1-z)^2 - l^2(1-2\cos^2\varphi)} \right], \quad (\text{B16})$$

or in particular Eq. (4) of the main text in the zero total momentum sector $l = 0$, while the dynamically constant energy shift in Eq. (B15) corresponds, up to $\mathcal{O}(N^{-1})$ -corrections, to the MF ground state energy per particle $-\tilde{\alpha}N/4$ one finds in the subcritical regime when solving the non-linear Schrödinger equation [74, 81] corresponding to the continuous model (A2).

The scaled version (B16) does not depend on \tilde{N} anymore. The scaled variables (B14) can therefore be considered the natural variables characterizing the physics. This means that *i*) the coupling strength α and *ii*) the momentum per particle l are the correctly scaled parameters characterizing the physical situation, and that *iii*) the homogeneous condensate fraction z , its conjugated coordinate φ and their dynamics are classically determined by only those two constants α and l and do not depend on the number of bosons N explicitly. The influence of N on the physics then takes place purely on the quantum level through its role as the effective quantum of action $\hbar_{\text{eff}} = 1/\tilde{N}$.

Appendix C: The asymptotic closure of the spectral gap

In the limit $N \rightarrow \infty$ low-lying excitation energies, described as quasi-particle excitations within Bogoliubov approximation [82–84], collapse to zero at criticality $\alpha = 1$. In the truncated three-site model they correspond to a linearization of the MF dynamics [governed by Eq. (4) of the main text] around the MF ground state, given by the upper boundary $z = 1$ or the stable fixed point in the sub- or supercritical regime, respectively. The associated frequency and thus the energy of the associated Bogoliubov quasiparticle vanish due to the bifurcation at $\alpha = 1$.

For any finite number $N < \infty$, however, the linearized description breaks down while the anharmonicity becomes dominant at criticality. To describe the resulting finite excitation gap $E_{\text{gap}} = \min_{\alpha}\{E_1 - E_0\}$ it is essential to account for this nonlinearity, which the analytic semiclassical quantization (6) is fully capable of [see Fig. 2 of the main text]. In the following we analyze the asymptotic closing of the spectral gap E_{gap} and the coupling $\alpha_{\text{gap}} = 1 + \Delta\alpha_{\text{gap}}$ at which it takes the smallest value.

At the gap $\alpha = \alpha_{\text{gap}}$ the involved ground state and first excited state are in the semiclassical picture always represented by a quantized vibration $\omega < 0$ and a quantized rotation $\omega > 0$, respectively. The separatrix action at the gap situation therefore is bounded by

$$\frac{1}{2\tilde{N}} < \frac{1}{2\pi} \oint d\varphi [1 - z(0, \varphi)] < \frac{3}{2\tilde{N}} \quad (\text{C2})$$

and thus has to vanish for $N \rightarrow \infty$, which naturally implies that α_{gap} approaches unity in the MF limit. We therefore consider

$$A = 1 - \alpha^{-1} > 0 \quad (\text{C3})$$

as a small parameter. In this regime the separatrix becomes parabolic

$$1 - z(0, \varphi) \approx \frac{8}{7}A \left(1 - \frac{\varphi^2}{A} \right) \quad (\text{C4})$$

between the unstable fixed points $|\varphi| \leq \sqrt{A}$. Since also the ground and first excited state are dominated by the separatrix region, Eq. (C4) indicates that for this discussion it is sufficient to consider the local phase space around $(z, \varphi) = (1, 0)$ with $1 - z = \mathcal{O}(A)$ and $\varphi = \mathcal{O}(\sqrt{A})$. In fact, after introducing scaled variables

$$\zeta = \frac{7}{4A}(1 - z), \quad \phi = \frac{1}{\sqrt{A}}\varphi, \quad (\text{C5})$$

one finds the local Hamilton function

$$\eta(\zeta, \phi) = \frac{\omega}{|\omega_{\text{min}}|} = \zeta^2 - 2\zeta(1 - \phi^2) + \mathcal{O}(A), \quad (\text{C6})$$

here normalized by the MF ground state energy

$$\omega_{\min} = -\frac{2}{7}\alpha(1 - \alpha^{-1})^2. \quad (\text{C7})$$

The scaling implies a major simplification to the problem and expresses a crucial low energy property of the system close to criticality. The dependence on the coupling α is absorbed into a pure rescaling of the MF degrees of freedom while the subdominant $\mathcal{O}(A)$ term in (C6) contains any residual dependence on the parameter α , irrelevant for the lowest states in the asymptotic regime $\alpha \approx 1$. This scaling behavior immediately implies that at $\alpha = \alpha_{\text{gap}}$ the scaled energies η_{vib} and η_{rot} of the two lowest states are universal constants and the gap energy thus scales as $E_{\text{gap}}/N \sim |\omega_{\min}| \sim A^2$. Further, the scaling exponent of α_{gap} with N can be readily taken from the parabolic form of the separatrix (C4), which, when integrated, gives an action S_{sep} that scales as $S_{\text{sep}} \sim A^{3/2}$ on the one hand. On the other hand it scales as $S_{\text{sep}} \sim 1/N$ at the gap situation $\alpha = \alpha_{\text{gap}}$ due to the bound (C2). Without further explicit calculation one thus finds

$$\Delta\alpha_{\text{gap}} \sim N^{-2/3}, \quad E_{\text{gap}} \sim N^{-1/3}, \quad (\text{C8})$$

giving analytical substantiation to the exponents observed in numerical calculations [46].

Furthermore, we can give analytical estimates for the universal coefficients that govern the asymptotic gap closing (C8). Based on the dominant local Hamilton function (C6) the distance of a rotation ($\eta > 0$) to the separatrix is given by

$$\delta\zeta_{\text{rot}}(\eta, \phi) = \sqrt{(1 - \phi^2)^2 + \eta} - |1 - \phi^2|, \quad (\text{C9})$$

while

$$\delta\zeta_{\text{vib}}(\eta, \phi) = 2\sqrt{(1 - \phi^2)^2 + \eta} \quad (\text{C10})$$

describes the distance between the upper and lower half-cycle of a vibration ($\eta < 0$). We define scaled action integrals

$$I(\eta) = \oint d\phi \zeta(\eta, \phi) \quad (\text{C11})$$

which, consistent with Eq. (6) of the main text, obey the semiclassical quantization condition

$$I(\eta_m) = \frac{7}{4}\pi A^{-3/2} \frac{1}{\tilde{N}} \left(m + \frac{1}{2} \right). \quad (\text{C12})$$

The action between a low lying rotation ($\eta > 0$) and the separatrix ($\eta = 0$) close to criticality is asymptotically given by

$$\delta I_{\text{rot}}(\eta) = \int_0^\infty d\phi \left(\sqrt{(1 - \phi^2)^2 + \eta} - |1 - \phi^2| \right). \quad (\text{C13})$$

Note that extending the upper integration limit to infinity does neither contradict with the finiteness of φ nor with the small angle approximation contained in (C6), since the integrand (C9) has a converging $\mathcal{O}(\phi^{-2})$ tail. Similarly, the scaled action integral of a vibration inside the separatrix island ($\eta < 0$) reads

$$I_{\text{vib}}(\eta) = 2 \int_0^{\sqrt{1 - \sqrt{-\eta}}} d\phi \sqrt{(1 - \phi^2)^2 + \eta}, \quad (\text{C14})$$

while the separatrix itself encloses the scaled area $I_{\text{sep}} = \frac{4}{3}$.

Because of the asymptotic scaling the quantization condition (C12), when applied to the scaled actions (C13) and (C14), can be formulated with just one free (dimensionless) parameter q instead of the two free parameters \tilde{N} and α , which had independent influence in the first place. This parameter should determine the physical situation, meaning it should reflect where exactly the system is located within the cross-over between the two separatrix-transitions of the ground state and the first excited state. A convenient choice is to define q as the area fraction of the vibrational orbit compared to the separatrix. With this choice the quantization conditions read

$$\begin{aligned} I_{\text{vib}}(\eta_{\text{vib}}) &= \frac{4}{3}q, \\ \delta I_{\text{rot}}(\eta_{\text{rot}}) &= 4q - \frac{4}{3}. \end{aligned} \quad (\text{C15})$$

The explicit relation between α , \tilde{N} and q is given by

$$A = 1 - \frac{1}{\alpha} = \left(\frac{21\pi}{32} \frac{1}{q\tilde{N}} \right)^{2/3}. \quad (\text{C16})$$

The meaningful values of q vary between $\frac{1}{3}$ and 1, corresponding to the transition of the rotation to a vibration and vice-versa. Inverting (C15) after the explicit use of (C13) and (C14) yields then two functions $\eta_{\text{rot}}(q)$ and $\eta_{\text{vib}}(q)$ that otherwise are independent of any system parameter. The gap energy (per particle) is

$$\begin{aligned} \Delta\omega(q) &= |\omega_{\min}(q)| \Delta\eta(q), \quad \text{with} \\ \Delta\eta(q) &= \eta_{\text{rot}}(q) - \eta_{\text{vib}}(q). \end{aligned} \quad (\text{C17})$$

There is still an additional explicit \tilde{N} -dependence in $\omega_{\min}(q)$, but it factorizes out in the regime of asymptotic scaling as

$$|\omega_{\min}(q)| = \frac{2}{7} \frac{A^2}{1 - A} \approx \frac{2}{7} A^2 \propto \tilde{N}^{-4/3} q^{-4/3}. \quad (\text{C18})$$

The condition $\frac{d}{dq} \log \Delta\omega(q) = 0$ at the gap (while $\tilde{N} = \text{const}$) translates to

$$\frac{d}{dq} \log \Delta\eta(q) = -\frac{d}{dq} \log |\omega_{\min}(q)| \approx \frac{4}{3q}, \quad (\text{C19})$$

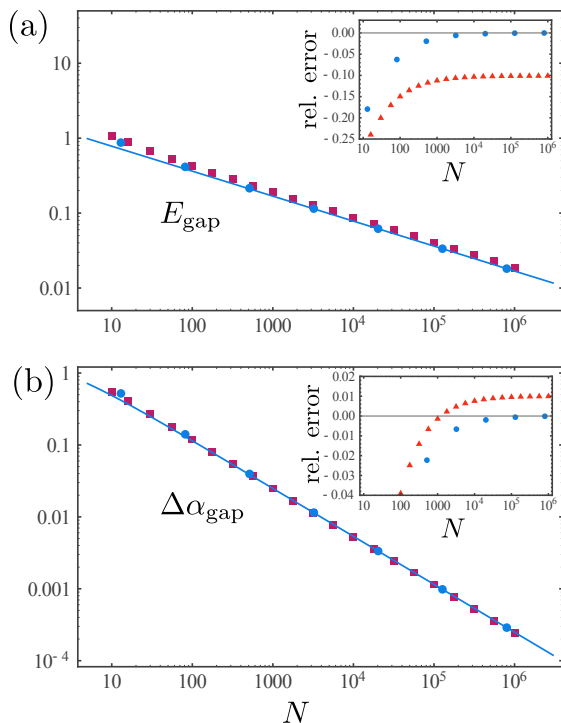


FIG. C1. (a) Gap energy E_{gap} and (b) correction $\Delta\alpha_{\text{gap}}$ to the gap location as a function of the number of particles. Asymptotic semiclassical results (C21) (solid blue), underlined by data obtained from the full semiclassical calculations (blue circles) and compared to numerical results obtained from exact diagonalization of the truncated model (purple squares). Insets: relative errors in the corresponding quantities of semiclassical asymptotics compared to full semiclassics (blue dots) and numerics (red triangles).

where in the last step the asymptotic expression in (C18) has been used. Solving (C19) for q determines the universal numerical constants

$$q_{\text{gap}}^{\text{scl}} = 0.525916\dots, \quad \Delta\eta_{\text{gap}}^{\text{scl}} = 0.953599\dots, \quad (\text{C20})$$

characterizing the finite-size QPT in the asymptotic limit $\tilde{N} \rightarrow \infty$ by semiclassical analysis. The semiclassical estimates for the finite size spectral gap and its location are

$$\begin{aligned} E_{\text{gap}} &= \tilde{N}|\omega_{\min}(q_{\text{gap}})|\Delta\eta_{\text{gap}} \approx 1.6841\dots \times N^{-1/3}, \\ \Delta\alpha_{\text{gap}} &\approx A(q_{\text{gap}}) \approx 2.4862\dots \times N^{-2/3}. \end{aligned} \quad (\text{C21})$$

In Fig. C1 we check the validity of the asymptotic semiclassical scalings (C21) by comparison with full semiclassics on the one hand to check the asymptotic analysis and with numerical calculations obtained from exact diagonalization on the other hand. While the deviation of the asymptotics from full semiclassics tends to zero for $N \rightarrow \infty$ as expected, a relative error of 10% and 1% in E_{gap} and $\Delta\alpha_{\text{gap}}$, respectively, when compared to numerics is persistent in this limit. This discrepancy stems from

the fact that here the system parameter α is changed during the limiting process $\hbar_{\text{eff}} = 1/\tilde{N} \rightarrow 0$ in a way that has a particularly strong impact on the classical-quantum correspondence. It is a direct consequence of the asymptotic scaling implied by the condition of staying at the minimum spectral gap. Despite the limit $N \rightarrow \infty$, the coupling is scaled in exactly such a way that the scale on which local nonlinearity has a significant influence on the classical dynamics is the same as the one of an effective Planck's cell. The former can be represented by the size of the separatrix, which, although defined as a purely classical action, is of the order of \hbar_{eff} , just because the parameter $\alpha = \alpha_{\text{gap}}$ is chosen appropriately.

On the one hand this insight clarifies that a semiclassical quantization is not capable of determining the coefficients in (C21) without error. On the other hand the semiclassical analysis lead to the asymptotic scaling of the phase space region relevant to the discussion on the spectral gap and can be used to overcome its own limitations by a requantization of the local asymptotic MF dynamics governed by (C6). A corresponding careful analysis [80] yields a quantum correction to the universal coefficients:

$$\begin{aligned} E_{\text{gap}}^{\text{quant}} &\approx 1.8688292(4)\dots \times N^{-1/3}, \\ \Delta\alpha_{\text{gap}}^{\text{quant}} &\approx 2.46016721(3)\dots \times N^{-2/3}. \end{aligned} \quad (\text{C22})$$

With these numbers, the numerical calculation of energy gaps by exact diagonalization cannot be distinguished from the asymptotics for large N anymore.

Appendix D: Universal separatrix quantization

In general, we focus on critical systems with an essentially one-dimensional description. In particular this applies to integrable systems by fixing $D - 1$ conserved quantities (like number of particles N and total momentum K in the truncated model considered in the main text), where D is the number of (collective) degrees of freedom. Nevertheless one can think of more general systems that become essentially one-dimensional around criticality whenever a clear scale separation allows for adiabatic treatment of additional degrees of freedom.

To be more specific, we focus on the supercritical regime and address local universal features in spectral and dynamical properties that are dominated by (highly) excited states close to transition. Whenever an excited state quantum phase transition (ESQPT) can be attributed to a separatrix crossing in the MF dynamics in effectively one dimension, which we consider as a generic mechanism for second order quantum phase transitions, a quantization condition similar to Eq. (6) of the main text applies in the semiclassical picture. For this we consider orbits on both sides close to a separatrix which translates to quantum states close to criticality for large N (small

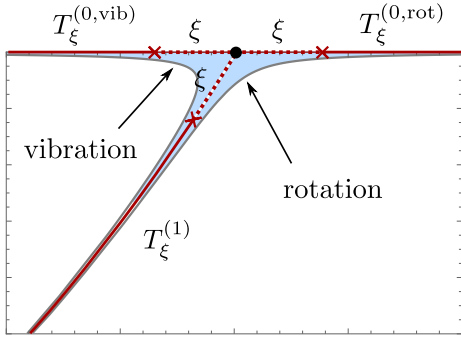


FIG. D1. Two orbits very close to the separatrix in energy. The corresponding orbit actions are dominated by the region around the saddle point (areas shown in light blue). Sub-dominant non-local contributions are given by on-separatrix traversal times $T_\xi^{(0,rot)}$, $T_\xi^{(0,vib)}$ and $T_\xi^{(1)}$ cut off at distances ξ from the hyperbolic fixed point.

\hbar_{eff}) while fixing the external parameter that drives the transition.

Although we are eventually interested in the application to critical MB systems, the following analysis is not restricted to this interpretation. Therefore we consider here any one-dimensional quantum system that derives from a quantization of a classical Hamiltonian system with a separatrix structure and write standard commutation relations as $[\hat{p}, \hat{q}] = -i\hbar$, which defines the meaning of \hbar in a specific context. While \hbar can be the actual Planck constant, it has to be reinterpreted as *effective* quantum of action $\hbar_{\text{eff}} \sim 1/N$ in the special case of MB systems, with MF dynamics formally defining the corresponding classical analogue.

For simplicity we set the classical energy, i.e., the Hamilton function $\omega(q, p)$, to $\omega = 0$ directly on the separatrix. In the limit $\hbar \rightarrow 0$ (or $N \rightarrow \infty$ in the MB context) the quantized energy levels close to $\omega = 0$ get arbitrarily small, allowing to use a specific local expansion of the Hamilton function $\omega(q, p)$ around the separatrix to determine the corresponding classical orbits. For this one has to realize that ω is quadratic at the saddle points where the separatrix intersects itself while it behaves only linearly on other parts of the separatrix. We thus split the corresponding action integrals into local parts close to the saddle points using a quadratic expansion there and non-local parts using linearization around the separatrix otherwise. The orbit actions (when defined relative to the separatrix) are dominated by the local regions around the hyperbolic fixed points while non-local parts of the separatrix give sub-dominant corrections as illustrated in Fig. D1 for the case of the specific model studied in the main text.

Consequently, a subsequent general semiclassical analysis reveals that the quantized levels close to $\omega = 0$ depend only on properties of the saddle point and the separatrix itself. We find general formulas for semiclassical

separatrix quantization, in the simplest form expressed as the smooth density of states

$$\bar{\rho}(\omega) = -\frac{1}{2\pi\hbar} \frac{1}{\lambda_\sigma} \log \frac{|\omega|}{\Omega} + \frac{t_\sigma^{\text{sep}}}{2\pi\hbar} + (\mu_< - \mu_>) \delta(\omega) + \mathcal{O}(\omega). \quad (\text{D2})$$

The corresponding discrete energy levels obtained by semiclassical action quantization around the ESQPT are [see Eq. (6) of the main text]

$$\omega_{[k]} \approx \frac{-2\pi\hbar\lambda_\sigma(\mu_\sigma + k)}{\mathcal{W}_{-1}(-2\pi\hbar\lambda_\sigma\Omega^{-1}e^{-1-\lambda_\sigma t_\sigma^{\text{sep}}})|\mu_\sigma + k|}, \quad k \in \mathbb{Z}, \quad (\text{D3})$$

ordered by k and with $\omega_{[0]}$ referring to the first level lying above the separatrix energy $\omega = 0$. In (D2) and (D3), \mathcal{W}_{-1} is the lower branch of the Lambert- \mathcal{W} function, which is the solution to $\mathcal{W}(x)e^{\mathcal{W}(x)} = x$ with $x \in [-e^{-1}, 0[$ and $\mathcal{W}_{-1}(x) \leq -1$. The inverse total stability exponent $\lambda^{-1} = \sum_j 1/\lambda^{(j)}$ is the sum of reciprocal stability exponents of all saddle points j involved. We introduced a typical classical (i.e., independent of \hbar) unit of energy Ω that characterizes the breakdown of the involved expansions of the classical Hamilton function. As a local approximation, Eq. (D3) is valid as long as $\omega_{[k]}/\Omega \ll 1$. The expressions (D2) and (D3) finally do not depend on the specific choice of Ω as the regularized separatrix traversal time t^{sep} is given by

$$t^{\text{sep}} = T^{\text{conv}} - \sum_j \frac{1}{\lambda^{(j)}} \log \left(\frac{\Omega}{2} \left(\frac{1}{\lambda_+^{(j)}} + \frac{1}{|\lambda_-^{(j)}|} \right) \right), \quad (\text{D4})$$

where $\lambda_\pm^{(j)}$ are the positive and negative eigenvalues of the Hessian when expanding the Hamiltonian around the saddle point j and

$$T^{\text{conv}} := \lim_{\xi \rightarrow 0} \left(T_\xi + \frac{2}{\lambda} \log \xi \right) \quad (\text{D5})$$

is the convergent part of the separatrix traversal time, with T_ξ the sum of on-separatrix traversal times cut off at (phase-space-) distances ξ from all involved saddle-points. To calculate the non-local constant t^{sep} in a specific system one has to give meaning to λ_\pm and phase space distance ξ , which are actually ill-defined objects because in general a phase space in Hamiltonian mechanics does not have a metric but rather a symplectic form (Note that in contrast, λ is well defined). To do the calculation one has to define arbitrary units q_0 of length and p_0 of momentum to get a dimensionless phase-space. The meaning of λ_\pm and ξ are then defined in that space (using Euclidean norm) with the outcome t^{sep} not depending on the particular choice of q_0 and p_0 . The constant index shifts $\mu_\sigma \in [0, 1[$ are related to the Maslov index and separatrix action. The index

$$\sigma = \begin{cases} < : \omega < 0 \\ > : \omega > 0 \end{cases} = \begin{cases} < : k < 0 \\ > : k \geq 0 \end{cases} \quad (\text{D6})$$

was introduced to indicate on which side of the separatrix the corresponding orbit lives, which may in principle involve different saddle-points and separatrix-segments, hence the distinction in λ , t^{sep} and μ . If $\mu_{<} = \mu_{>} \equiv \mu$ we will call the quantized orbits “smoothly connected” through the transition.

The dominant term $\sim \log |\omega|$ in Eq. (D2) determined locally by only the saddle point has been found before (see [39] for a corresponding classification of ESQPTs) by counting the reduction of classical phase space volumes due to potential energy maxima. In contrast, the subdominant terms, non-locally determined by properties of the whole separatrix, are, to the best of our knowledge, original. More importantly, the discrete levels (D3) not only describe the local spectrum on average, as given by Eq. (D2). Equation (D3) may indeed be obtained from Eq. (D2) by effective quantization $\int_{0^+}^{\omega_{[k]}} d\omega \bar{\rho}(\omega) = \mu_{>} + k$ of the average density of states. Moreover, the form (D3) has been noted [37] in a corresponding analysis. However, in the analysis presented here it represents by no means just an artificially constructed, maximally uniform spectrum consistent with $\bar{\rho}$. Instead, Eq. (D3) gives the actual individual levels obtained by applying the full semi-classical quantization condition as in Eq. (6) of the main text, as long as $\omega_{[k]}/\Omega \ll 1$. The local spectrum thus is indeed as uniform as possible, absent of any fluctuations. This is due to the one-dimensional description and has the far reaching consequence of asymptotically constant level spacing (see Appendix F).

Appendix E: Separatrix quantization in the model

Using the scaled phase space variables [Eq. (5) of the main text] and scaled Hamiltonian (energy per particle) $\omega(z, \varphi)$ [Eq. (4) of the main text] gives the Hessian

$$\mathcal{H} = \begin{pmatrix} 0 & -2\sqrt{\alpha-1} \\ -2\sqrt{\alpha-1} & 2 - \frac{\alpha}{4} \end{pmatrix} \quad (\text{E2})$$

at the hyperbolic fixed point (here chosen to be the one located at $\varphi > 0$). Due to symmetry the corresponding stability exponent $\lambda^{(j)} = \sqrt{-\det \mathcal{H}} = 2\sqrt{\alpha-1}$ is the same for both fixed points $j = 1, 2$. The total exponent determining the dominant spacing [see Eq. (7) of the main text] is therefore

$$\lambda = \sqrt{\alpha-1}, \quad (\text{E3})$$

while for the subdominant contribution t the eigenvalues of \mathcal{H} give

$$\frac{1}{2} \left(\frac{1}{\lambda_+^{(j)}} + \frac{1}{|\lambda_-^{(j)}|} \right) = \frac{\sqrt{(1 - \frac{\alpha}{8})^2 + 4(\alpha-1)}}{4(\alpha-1)}. \quad (\text{E4})$$

For the separatrix traversal times the separatrix can be split into three segments (see Fig. D1), defining the

traversal times *i*) $T_\xi^{(0,\text{rot})}$ for the outer upper boundary at $\cos^2 \varphi < 1/\alpha$ for rotations, *ii*) $T_\xi^{(0,\text{vib})}$ for the inner upper boundary at $\cos^2 \varphi > 1/\alpha$ for vibrations and *iii*) $T_\xi^{(1)}$ for the curved separatrix segment between the two saddle points separating vibrations and rotations. We calculate the traversal times as

$$T_\gamma = \int_{\mathcal{C}_\gamma} d\varphi \left| \frac{\partial \omega}{\partial z} \right|_{\mathcal{C}_\gamma}^{-1} \quad (\text{E5})$$

along the corresponding segment \mathcal{C}_γ . The first segment, which connects the two fixed points by going over $\varphi = \pi/2 \equiv -\pi/2 \pmod{\pi}$, gives

$$T_\xi^{(0,\text{rot})} = 2 \int_{\arccos \frac{1}{\sqrt{\alpha}} + \xi}^{\frac{\pi}{2}} d\varphi (1 - \alpha \cos^2 \varphi)^{-1}, \quad (\text{E6})$$

which can be elementarily integrated to yield

$$T_\xi^{(0,\text{rot})} = -\frac{1}{\sqrt{\alpha-1}} \left[\log \xi + \log \left(\frac{2}{\alpha} \sqrt{\alpha-1} \right) \right] + \mathcal{O}(\xi), \quad (\text{E7})$$

containing the convergent part

$$T_{\text{conv}}^{(0,\text{rot})} = \frac{1}{\sqrt{\alpha-1}} \log \left(\frac{2}{\alpha} \sqrt{\alpha-1} \right). \quad (\text{E8})$$

An analogous calculation gives exactly the same for the vibration-related boundary segment

$$T_\xi^{(0,\text{vib})} = T_\xi^{(0,\text{rot})}, \quad T_{\text{conv}}^{(0,\text{vib})} = T_{\text{conv}}^{(0,\text{rot})}. \quad (\text{E9})$$

The linearized energy $\partial \omega / \partial z$ takes the same form on the curved segment as for the upper boundary, thus

$$T_\xi^{(1)} = 2 \int_0^{\arccos \frac{1}{\sqrt{\alpha}} - \Delta \varphi_\xi} d\varphi (\alpha \cos^2 \varphi - 1)^{-1}. \quad (\text{E10})$$

The cut-off in φ , denoted by $\Delta \varphi_\xi$ is related to the Euclidean phase space distance ξ along the tilted segment by

$$\Delta \varphi_\xi = \frac{\xi}{\sqrt{1 + \left(\frac{dz^{(\text{sep})}}{d\varphi} \right)_{\text{FP}}^2}} = \frac{1 - \frac{\alpha}{8}}{\sqrt{(1 - \frac{\alpha}{8})^2 + 4(\alpha-1)}} \xi. \quad (\text{E11})$$

The traversal time is then given by

$$T_\xi^{(1)} = -\frac{1}{\sqrt{\alpha-1}} \log \xi + T_{\text{conv}}^{(1)} + \mathcal{O}(\xi), \quad (\text{E12})$$

with its convergent part

$$T_{\text{conv}}^{(1)} = \frac{1}{\sqrt{\alpha-1}} \log \left(\frac{2}{\alpha} \sqrt{\alpha-1} \right) + \frac{1}{\sqrt{\alpha-1}} \log \left(\frac{\xi}{\Delta \varphi_\xi} \right). \quad (\text{E13})$$

The second term in (E13) essentially compensates (E4) in the total regularized separatrix traversal time (D4) and

may be associated with the specific choice of phase space coordinates and Euclidean norm that drops out eventually. The regularized separatrix traversal time reads,

$$t^{\text{sep}} = \frac{1}{\sqrt{\alpha-1}} \log\left(\frac{128(\alpha-1)^2}{\alpha^2(8-\alpha)}\right) \quad (\text{E14})$$

on both sides of the transition.

Altogether, combining (E14), (E3) and (D2), the asymptotic DoS $\bar{\rho}(E) = \bar{\rho}(\omega)/N$ close to the ESQPT is given by Eq. (7) of the main text.

Appendix F: Asymptotic spectral equidistance

Considering the formal semiclassical limit $\hbar \rightarrow 0$ in (D3) by application of the asymptotics $\mathcal{W}_{-1}(x) = \log(-x) - \log(-\log(-x)) + \mathcal{O}[\log(-\log(-x))/\log(-x)]$ results in the universal asymptotic law

$$\omega_{[k]} \sim 2\pi\hbar\lambda_\sigma \left(\log\frac{s_0}{\hbar}\right)^{-1} (\mu_\sigma + k) \times \left(1 + \mathcal{O}\left(\frac{\log\log\frac{s_0}{\hbar}}{\log\frac{s_0}{\hbar}}\right)\right) \quad (\text{F2})$$

of constant level spacing that depends only on the stability exponents associated with involved saddle-points. Here, s_0 is an arbitrarily chosen but classically defined (typical) action of the system, merely introduced to maintain proper units while asymptotically irrelevant.

If $\lambda_< = \lambda_> \equiv \lambda$ the asymptotic level spacing (F2) induces the single Ehrenfest-like time scale [see Eq. (9) of the main text]

$$\tau \sim \frac{1}{\lambda} \log\frac{s_0}{\hbar} \quad (\text{F3})$$

for quantum mechanical processes that dominantly involve the states in the band of high DoS around the separatrix energy $\omega = 0$.

There is, however, a subtle constraint involved in the asymptotic expressions (F2) and (F3), for which the quantum number k was assumed to be fixed during the limiting process. For a dynamical process, however, typically the number of dominantly involved states also grows with s_0/\hbar . Therefore one has to address the question of how many states around the separatrix, as a function of \hbar , can be considered asymptotically equidistant. Let $K = K(\hbar)$ denote this number. We presume $\lim_{\hbar \rightarrow 0} \hbar K(\hbar) = 0$, as implied by the prerequisite $\lim_{\hbar \rightarrow 0} \omega_{[K(\hbar)]} = 0$ necessary for the close-to-separatrix quantization (D2) and (D3). As indicator for equidistance we consider the mean level spacing $\langle \Delta\omega \rangle_K = \omega_{[K]}/K$ averaged over $K(\hbar)$ states lying against $\omega = 0$. Based on (D3) the asymptotics for \mathcal{W}_{-1} give

$$\langle \Delta\omega \rangle_K = \frac{2\pi\hbar\lambda}{\log\frac{s_0}{\hbar} - \log K(\hbar)} \times \left(1 + \mathcal{O}\left(\frac{\log\log\frac{s_0}{\hbar K}}{\log\frac{s_0}{\hbar K}}\right)\right). \quad (\text{F4})$$

If the number of levels $K(\hbar)$ is irrelevant to the level spacing we identify asymptotic equidistance. In view of (F4)

this poses the constraint $\lim_{\hbar \rightarrow 0} \log K(\hbar)/\log(s_0/\hbar) = 0$, which is equivalent to a sub-algebraic scaling of involved states, i.e.,

$$(\forall \nu > 0) \left(\lim_{\hbar \rightarrow 0} \left(\frac{\hbar}{s_0}\right)^\nu K(\hbar) = 0 \right), \quad (\text{F5})$$

since only then the K -dependent part in the denominator of Eq. (F4) becomes subdominant compared to $\log(s_0/\hbar)$.

Appendix G: Quench dynamics of inter-particle correlations—the finite-size corrected log time

Close to criticality $E \approx E_{\text{sep}}$, the eigenstates of the bosonic system described by (A9) in the supercritical regime $\alpha > 1$ are far from pure condensates with all atoms occupying a single but arbitrary mode. The associated inter-particle correlations can be quantified by the von Neumann entropy

$$S = -\text{Tr}(\hat{\rho} \log \hat{\rho}) \quad (\text{G2})$$

of the 3×3 reduced one-body density matrix (ROBDM)

$$\rho_{kl} = \frac{1}{N} \langle \psi | \hat{a}_k^\dagger \hat{a}_l | \psi \rangle \quad (\text{G3})$$

of a pure state $|\psi\rangle$.

To study entanglement spreading as another facet of quantum information scrambling we consider (as in [56]) the evolution of $S(t)$ after the quantum quench, where the non-interacting ground state, i.e., the pure condensate $|\psi(t=0)\rangle = 1/\sqrt{N!}(\hat{a}_0^\dagger)^N|0\rangle$, evolves subject to the interacting Hamiltonian (A9) with $\alpha > 1$. Eq. (G2) expresses inter-particle correlations as loss of information when all but one particles are traced out. An initial increase of $S(t)$ after the quench thus represents a form of information scrambling, similar to the increase of the OTOC [Eq. (10) of the main text]: While the latter quantifies the scrambling of information among sites or modes, the former quantifies scrambling among *particles*.

Because of total momentum conservation $[\hat{K}, \hat{\mathcal{H}}] = 0$ in the considered system, the ROBDM takes a very simple form. The time-evolved state becomes

$$|\psi(t)\rangle = \sum_{m=0}^{\frac{N}{2}} c_m(t) |m, N-2m, m\rangle \quad (\text{G4})$$

(with N even for simplicity), represented in Fock basis

$$|m_{-1}, m_0, m_1\rangle \equiv \frac{(\hat{a}_{-1}^\dagger)^{m_{-1}} (\hat{a}_0^\dagger)^{m_0} (\hat{a}_1^\dagger)^{m_1}}{\sqrt{m_{-1}! m_0! m_1!}} |0\rangle, \quad (\text{G5})$$

where $|0\rangle$ denotes the vacuum of $N = 0$ particles. Because the operator $\hat{a}_k^\dagger \hat{a}_l$ cannot change three occupation numbers simultaneously, its matrix elements are restricted to

$$\langle n, N-2n, n | \hat{a}_k^\dagger \hat{a}_l | m, N-2m, m \rangle \propto \delta_{nm} \delta_{kl}. \quad (\text{G6})$$

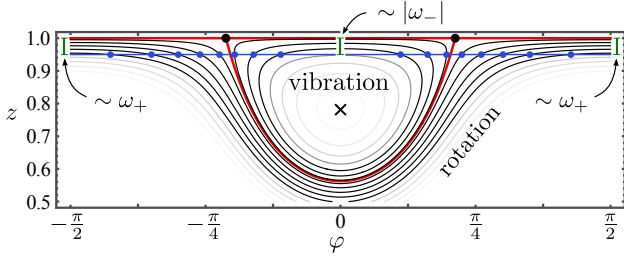


FIG. G1. Librations and rotations (black) in the vicinity of the separatrix are intersecting (blue dots) the horizontal line corresponding to the non-interacting ground state (blue solid). Non-intersecting orbits are grayed out to indicate exponentially suppressed overlaps. The criterion for intersection depends on the peak value of z located at $\varphi = \pm\frac{\pi}{2}$ (rot.) or $\varphi = 0$ (vib.), where $\omega(z, \varphi)$ can be linearized in z and therefore $1 - z = 1/(2\tilde{N}) \sim |\omega_{\pm}|$.

This results in the diagonal form

$$\hat{\rho}(t) = \frac{1}{N} \begin{pmatrix} \langle m_{\pm 1} \rangle_t & 0 & 0 \\ 0 & N - 2\langle m_{\pm 1} \rangle_t & 0 \\ 0 & 0 & \langle m_{\pm 1} \rangle_t \end{pmatrix}, \quad (\text{G7})$$

depending only on the expectation value $\langle m_{\pm 1} \rangle_t = \sum_m |c_m(t)|^2 m$ of the $k = \pm 1$ momentum mode occupation.

When represented in the energy eigenbasis $\{|n\rangle\}$ of the interacting system, the ROBDM reads

$$\rho_{kl}(t) = \frac{1}{N} \sum_{n,m} d_n^* d_m \langle n | \hat{a}_k^\dagger \hat{a}_l | m \rangle e^{-i(E_m - E_n)t}, \quad (\text{G8})$$

where $d_n = \langle n | \psi(0) \rangle$. States in the vicinity of the ES-QPT are dominantly involved in the process, because $|\psi(0)\rangle$ corresponds to the classical orbit given by the horizontal line $z = 1 - 1/(2\tilde{N})$, very close to the upper boundary of the phase space. A semiclassical estimate of the number of states around the separatrix that are dominantly involved is given by the criterion that the corresponding orbits intersect this horizontal line as depicted in Fig. G1. This is because the overlap d_n typically drops off exponentially for states $|n\rangle$ whose corresponding quantized orbits are beyond intersection, analogous to the exponential decay of WKB wave functions in classically forbidden regions. From a linearization of $\omega(z, \varphi)$ at $(z, \varphi) = (1, \pi/2)$ and $(z, \varphi) = (1, 0)$, valid for large N , one gets the corresponding bound $\omega_- < \omega < \omega_+$ with $\omega_- = -(\alpha - 1)/\tilde{N}$ and $\omega_+ = 1/\tilde{N}$, both scaling as $\omega_{\pm} \sim 1/\tilde{N}$. In view of (F2) the number of dominantly contributing states thus scales subalgebraically as

$$K \sim |\omega_{\pm}| \tilde{N} \log \tilde{N} \sim \log N, \quad (\text{G9})$$

justifying the use of (F2) in the first place and fulfilling the requirement (F5) for asymptotically constant level spacing. While for exactly equidistant energies

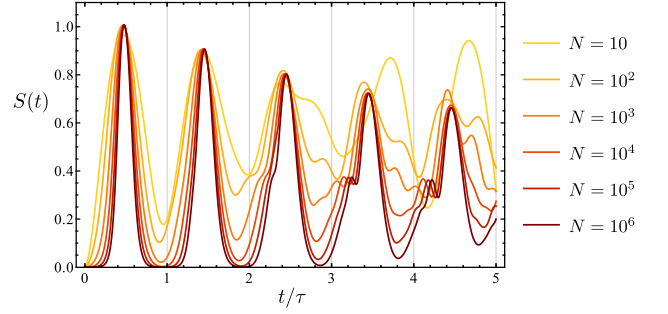


FIG. G2. Evolution of the von Neumann entropy (G2) of the ROBDM (G2) initialized in the non-interacting ground state numerically calculated for $\alpha = 2$ and $N = 10^n$ with $n = 1, 2, 3, 4, 5, 6$. The increasing quality of periodicity with growing N is in particular reflected in the improvement of revivals $S(j\tau) \approx 0$ for $j \in \mathbb{N}$. The time is scaled with the (pseudo-)period τ (G11) associated with the estimate for the average involved level-spacing.

$E_m - E_n = (m - n)\Delta E$ the ROBDM (G8) becomes periodic in time with period $\tau = 2\pi/\Delta E$, this periodicity is flawed for finite N , resulting in only partial recurrence, because neither is the spectrum exactly equidistant for dominantly contributing states, nor can states with larger $|\omega| > |\omega_{\pm}|$ be fully ignored. When increasing N the periodicity should slowly become more and more perfect. This tendency is demonstrated in figure Fig. G2.

For finite N one can estimate the correction to the characteristic time scale by averaging the inverse level-spacing $\Delta\omega^{-1} = 1/\bar{\rho}(\omega)$ over the interval $\omega \in [\omega_-, \omega_+]$ assuming constant weight:

$$\langle \Delta\omega^{-1} \rangle \approx \frac{1}{\omega_+ - \omega_-} \int_{\omega_-}^{\omega_+} d\omega \bar{\rho}(\omega), \quad (\text{G10})$$

which results in the estimated time scale

$$\tau = \frac{1}{\sqrt{\alpha - 1}} \left[\log N + 1 + \log \left(\frac{128(\alpha - 1)^2}{\alpha^2(8 - \alpha)} \right) - \frac{\alpha - 1}{\alpha} \log(\alpha - 1) \right]. \quad (\text{G11})$$

Since (G11) is the characteristic time scale of the whole evolution of $S(t)$, it directly determines the scrambling time τ_{scr} , which refers to the initial growth. Defined by the condition $S(\tau_{\text{scr}}) = S_{\text{th}}$ with some arbitrary, small valued threshold entropy S_{th} , the scrambling time asymptotically becomes

$$\tau_{\text{scr}} = \text{const.} \times \frac{1}{\sqrt{\alpha - 1}} \log N + \mathcal{O}(1). \quad (\text{G12})$$

The logarithmic scaling with N as a numerical observation has already been reported in Ref. [56], where also a general connection to an instability has been suspected. The semiclassical treatment presented here provides sufficient analytical ground for supplying those

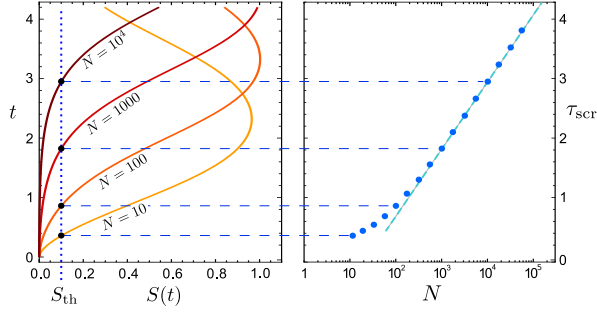


FIG. G3. Scrambling times τ_{scr} for $\alpha = 2$ obtained from numerically evolved entropies $S(t)$ (G2) using the threshold $S_{\text{th}} = 0.1$ for several numbers of particles (left). Plotting those against N logarithmically (right) shows a linear dependence on $\log N$ for $N \gtrsim 100$, confirming the scaling in Eq. (G12). The prefactor and additive constant are fitted (dashed).

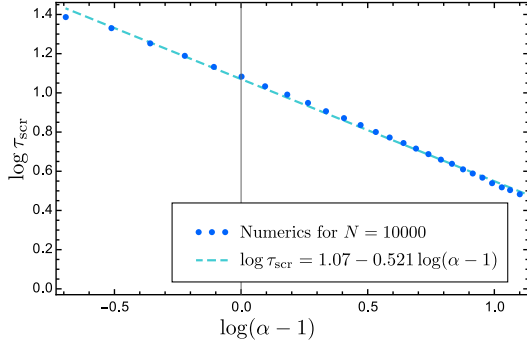


FIG. G4. Numerical scrambling times obtained as in Fig. G3 for $N = 10^4$ as a function of α . A linear fit to the doubly logarithmic data supports the predicted dominant scaling with $\sqrt{\alpha - 1}$ (G12). Deviations thereof (small mismatch in the exponent 0.521 from the prediction 0.5 and additional functional dependence on α) are attributed to finite-size effects expected to vanish asymptotically.

statements with explicit analytical expressions and thorough derivation. Furthermore, the one-to-one correspondence between $S(t)$ and the mean condensate fraction $\langle \psi | \hat{n}_0(t) | \psi \rangle / N$, as evident from (G7), establishes a connection to Ref. [85], where oscillatory behavior has been reported based on a quasi-classical picture valid for times up to τ_E . While the classical phase space sampling used in [85] infers decaying oscillations of $S(t)$, unitary quantum evolution, implemented in our approach (6), implies strong revivals, periodically leading to $S(t) \approx 0$ beyond τ_E . Eventually, for $N \rightarrow \infty$, the quantum and quasi-classical picture become unified again, due to the peculiarity of asymptotic spectral equidistance, analogous to harmonic oscillator levels, where a quasi-classical description would become exact. Finally, Figs. G3 and G4 show numerical confirmation of (G12).

- [1] E. Altman, *Nat. Phys.* **14**, 979 (2018).
- [2] B. Swingle, *Nat. Phys.* **14**, 988 (2018).
- [3] M. Srednicki, *Phys. Rev. E* **50**, 888 (1994).
- [4] M. Rigol, V. Dunjko, and M. Olshanii, *Nature* **452**, 854 (2008).
- [5] J. Eisert, M. Friesdorf, and C. Gogolin, *Nat. Phys.* **11**, 124 (2015).
- [6] A. M. Kaufman, M. E. Tai, A. Lukin, M. Rispoli, R. Schittko, P. M. Preiss, and M. Greiner, *Science* **353**, 794 (2016).
- [7] R. Nandkishore and D. A. Huse, *Annu. Rev. Condens. Matter Phys.* **6**, 15 (2015).
- [8] M. Schreiber, S. S. Hodgman, P. Bordia, H. P. Lüschen, M. H. Fischer, R. Vosk, E. Altman, U. Schneider, and I. Bloch, *Science* **349**, 842 (2015).
- [9] A. I. Larkin and Y. N. Ovchinnikov, *J. Exp. Theor. Phys.* **28**, 1200 (1969).
- [10] J. Maldacena, S. H. Shenker, and D. Stanford, *J. High Energy Phys.* **2016**, 106 (2016).
- [11] J. Maldacena and D. Stanford, *Phys. Rev. D* **94**, 106002 (2016).
- [12] M. Gärttner, J. G. Bohnet, A. Safavi-Naini, M. L. Wall, J. J. Bollinger, and A. M. Rey, *Nat. Phys.* **13**, 781 (2017).
- [13] J. Li, R. Fan, H. Wang, B. Ye, B. Zeng, H. Zhai, X. Peng, and J. Du, *Phys. Rev. X* **7**, 031011 (2017).
- [14] K. X. Wei, C. Ramanathan, and P. Cappellaro, *Phys. Rev. Lett.* **120**, 070501 (2018).
- [15] Y. Chen, “Universal logarithmic scrambling in many body localization,” (2016), arXiv:1608.02765.
- [16] Y. Huang, Y.-L. Zhang, and X. Chen, *Ann. Phys.* **529**, 1600318 (2017).
- [17] R. Fan, P. Zhang, H. Shen, and H. Zhai, *Sci. Bull.* **62**, 707 (2017).
- [18] B. Swingle and D. Chowdhury, *Phys. Rev. B* **95**, 060201 (2017).
- [19] B. Dóra and R. Moessner, *Phys. Rev. Lett.* **119**, 026802 (2017).
- [20] J. S. Cotler, G. Gur-Ari, M. Hanada, J. Polchinski, P. Saad, S. H. Shenker, D. Stanford, A. Streicher, and M. Tezuka, *J. High Energy Phys.* **2017**, 118 (2017).
- [21] A. Kitaev, (2015), talks at KITP, <http://online.kitp.ucsb.edu/online/entangled15/kitaev/>, <http://online.kitp.ucsb.edu/online/entangled15/kitaev2/>.
- [22] J. Polchinski and V. Rosenhaus, *J. High Energy Phys.* **2016**, 1 (2016).
- [23] A. A. Patel and S. Sachdev, *Proc. Natl. Acad. Sci. U.S.A.* **114**, 1844 (2017).
- [24] H. Shen, P. Zhang, R. Fan, and H. Zhai, *Phys. Rev. B* **96**, 054503 (2017).
- [25] M. Heyl, F. Pollmann, and B. Dóra, *Phys. Rev. Lett.* **121**, 016801 (2018).
- [26] Y. Alavirad and A. Lavasani, “Scrambling in the Dicke model,” (2018), arXiv:1808.02038.
- [27] J. Chávez-Carlos, B. López-del Carpio, M. A. Bastarrachea-Magnani, P. Stránský, S. Lerma-Hernández, L. F. Santos, and J. G. Hirsch, “Quantum and Classical Lyapunov Exponents in Atom-Field Interaction Systems,” (2018), arXiv:1807.10292.
- [28] B. Swingle, G. Bentsen, M. Schleier-Smith, and P. Hayden, *Phys. Rev. A* **94**, 040302 (2016).
- [29] E. B. Rozenbaum, S. Ganeshan, and V. Galitski, *Phys.*

- Rev. Lett. **118**, 086801 (2017).
- [30] A. Bohrdt, C. B. Mendl, M. Endres, and M. Knap, *New J. Phys.* **19**, 063001 (2017).
- [31] T. Scaffidi and E. Altman, “Semiclassical theory of many-body quantum chaos and its bound,” (2017), arXiv:1711.04768.
- [32] J. Rammensee, J. D. Urbina, and K. Richter, *Phys. Rev. Lett.* **121**, 124101 (2018).
- [33] I. García-Mata, M. Saraceno, R. A. Jalabert, A. J. Roncaglia, and D. A. Wisniacki, *Phys. Rev. Lett.* **121**, 210601 (2018).
- [34] S. Tomsovic, P. Schlagheck, D. Ullmo, J.-D. Urbina, and K. Richter, *Phys. Rev. A* **97**, 061606 (2018).
- [35] C. W. von Keyserlingk, T. Rakovszky, F. Pollmann, and S. L. Sondhi, *Phys. Rev. X* **8**, 021013 (2018).
- [36] C. Emary and T. Brandes, *Phys. Rev. E* **67**, 066203 (2003).
- [37] M. A. Caprio, P. Cejnar, and F. Iachello, *Ann. Phys.* **323**, 1106 (2008).
- [38] V. M. Bastidas, P. Pérez-Fernández, M. Vogl, and T. Brandes, *Phys. Rev. Lett.* **112**, 140408 (2014).
- [39] P. Stránský, M. Macek, and P. Cejnar, *Ann. Phys.* **345**, 73 (2014).
- [40] M. A. Bastarrachea-Magnani, S. Lerma-Hernández, and J. G. Hirsch, *J. Stat. Mech. Theory Exp.* **2016**, 093105 (2016).
- [41] D. Rubeni, J. Links, P. S. Isaac, and A. Foerster, *Phys. Rev. A* **95**, 043607 (2017).
- [42] S. Pappalardi, A. Russomanno, B. Žunkovič, F. Iemini, A. Silva, and R. Fazio, *Phys. Rev. B* **98**, 134303 (2018).
- [43] Such a harmonic oscillator-type spectrum has also been found for the special case of the xp model in AdS_2 [86].
- [44] Quantum recurrences in chaotic systems are exceptional and can exist only at particular wavelengths [87].
- [45] E. H. Lieb and W. Liniger, *Phys. Rev.* **130**, 1605 (1963).
- [46] R. Kanamoto, H. Saito, and M. Ueda, *Phys. Rev. A* **67**, 013608 (2003).
- [47] A. G. Sykes, P. D. Drummond, and M. J. Davis, *Phys. Rev. A* **76**, 063620 (2007).
- [48] K. E. Strecker, G. B. Partridge, A. G. Truscott, and R. G. Hulet, *Nature* **417**, 150 (2002).
- [49] L. Khaykovich, F. Schreck, G. Ferrari, T. Bourdel, J. Cubizolles, L. D. Carr, Y. Castin, and C. Salomon, *Science* **296**, 1290 (2002).
- [50] C. Chin, R. Grimm, P. Julienne, and E. Tiesinga, *Rev. Mod. Phys.* **82**, 1225 (2010).
- [51] R. Kanamoto, H. Saito, and M. Ueda, *Phys. Rev. Lett.* **94**, 090404 (2005).
- [52] R. Kanamoto, H. Saito, and M. Ueda, *Phys. Rev. A* **73**, 033611 (2006).
- [53] K. Sakmann, A. I. Streltsov, O. E. Alon, and L. S. Cederbaum, *Phys. Rev. A* **72**, 033613 (2005).
- [54] D. Flassig, A. Franca, and A. Pritzel, *Phys. Rev. A* **93**, 013627 (2016).
- [55] L. Piroli and P. Calabrese, *Phys. Rev. A* **94**, 053620 (2016).
- [56] G. Dvali, D. Flassig, C. Gomez, A. Pritzel, and N. Wintergerst, *Phys. Rev. D* **88**, 124041 (2013).
- [57] G. Dvali and M. Panchenko, “Black Hole Type Quantum Computing in Critical Bose-Einstein Systems,” (2015), arXiv:1507.08952.
- [58] G. Dvali and C. Gomez, *Eur. Phys. J. C* **74**, 2752 (2014).
- [59] C. S. Gerving, T. M. Hoang, B. J. Land, M. Anquez, C. D. Hamley, and M. S. Chapman, *Nat. Commun.* **3**, 1169 (2012).
- [60] G. Arwas, A. Vardi, and D. Cohen, *Sci. Rep.* **5**, 13433 (2015).
- [61] M. Prüfer, P. Kunkel, H. Strobel, S. Lannig, D. Linneemann, C.-M. Schmied, J. Berges, T. Gasenzer, and M. K. Oberthaler, *Nature* **563**, 217 (2018).
- [62] M. A. Garcia-March, S. van Frank, M. Bonneau, J. Schmiedmayer, M. Lewenstein, and L. F. Santos, *New J. Phys.* **20**, 113039 (2018).
- [63] A. Kosior, A. Syrwid, and K. Sacha, *Phys. Rev. A* **98**, 023612 (2018).
- [64] B. M. Herbst and M. J. Ablowitz, *Phys. Rev. Lett.* **62**, 2065 (1989).
- [65] M. Tabor, *Chaos and Integrability in Nonlinear Dynamics: An Introduction* (John Wiley & Sons, 1989).
- [66] A. M. Ozorio de Almeida, *Hamiltonian Systems: Chaos and Quantization* (Cambridge University Press, 1990).
- [67] T. Engl, J. Dujardin, A. Argüelles, P. Schlagheck, K. Richter, and J. D. Urbina, *Phys. Rev. Lett.* **112**, 140403 (2014).
- [68] M. Albiez, R. Gati, J. Fölling, S. Hunsmann, M. Cristiani, and M. K. Oberthaler, *Phys. Rev. Lett.* **95**, 010402 (2005).
- [69] R. Gati, M. Albiez, J. Fölling, B. Hemmerling, and M. K. Oberthaler, *Appl. Phys. B* **82**, 207 (2006).
- [70] E. M. Graefe and H. J. Korsch, *Phys. Rev. A* **76**, 032116 (2007).
- [71] R. M. Corless, G. H. Gonnet, D. E. G. Hare, D. J. Jeffrey, and D. E. Knuth, *Adv. Comput. Math.* **5**, 329 (1996).
- [72] G. Berman and G. Zaslavsky, *Physica A* **91**, 450 (1978).
- [73] B. Rauer, S. Erne, T. Schweigler, F. Cataldini, M. Tajik, and J. Schmiedmayer, *Science* **360**, 307 (2018).
- [74] Y. Castin, *J. Phys. IV France* **116**, 89 (2004).
- [75] M. Olshanii, *Phys. Rev. Lett.* **81**, 938 (1998).
- [76] Y. Nishida, *Phys. Rev. A* **97**, 061603 (2018).
- [77] L. Pricoupenko, *Phys. Rev. A* **97**, 061604 (2018).
- [78] G. Guijarro, A. Pricoupenko, G. E. Astrakharchik, J. Boronat, and D. S. Petrov, *Phys. Rev. A* **97**, 061605 (2018).
- [79] C. Gardiner and P. Zoller, *Quantum Noise: A Handbook of Markovian and Non-Markovian Quantum Stochastic Methods with Applications to Quantum Optics*, Springer Series in Synergetics (Springer Berlin, 2004).
- [80] Q. Hummel, *Semiclassical Theory of Few- and Many-body Quantum Systems with Short-range Interactions*, Ph.D. thesis, Universität Regensburg (2018).
- [81] L. Pitaevskii and S. Stringari, *Bose-Einstein Condensation and Superfluidity*, International Series of Monographs on Physics (Oxford University Press, 2016).
- [82] N. N. Bogoliubov, *J. Phys. (USSR)* **11**, 23 (1947).
- [83] P. G. de Gennes, *Superconductivity of Metals and Alloys*, Frontiers in Physics (W. A. Benjamin, 1966).
- [84] A. L. Fetter, *Ann. Phys. (New York)* **70**, 67 (1972).
- [85] R. Mathew and E. Tiesinga, *Phys. Rev. A* **96**, 013604 (2017).
- [86] J. Molina-Vilaplana and G. Sierra, *Nucl. Phys. B* **877**, 107 (2013).
- [87] S. Tomsovic and J. H. Lefebvre, *Phys. Rev. Lett.* **79**, 3629 (1997).